

Low-end mass function of the Quintuplet cluster

Jihye Shin^{1,2*} and Sungsoo S. Kim^{3,4†}

¹*Kavli Institute for Astronomy and Astrophysics at Peking University, Yi He Yuan Lu 5, Hai Dian District, Beijing 100871, P.R. China*

²*School of Physics, Korea Institute for Advanced Study, Heogiro 85, Seoul 02455, Republic of Korea*

³*Department of Astronomy & Space Science, Kyung Hee University, Yongin, Kyungki 17104, Republic of Korea*

⁴*School of Space Research, Kyung Hee University, Yongin, Kyungki 17104, Republic of Korea*

Accepted 1988 December 15. Received 1988 December 14; in original form 1988 October 11

ABSTRACT

The Quintuplet and Arches clusters, which were formed in the harsh environment of the Galactic Center (GC) a few million years ago, have been excellent targets for studying the effects of a star-forming environment on the initial mass function (IMF). In order to estimate the shape of the low-end IMF of the Arches cluster, Shin & Kim devised a novel photometric method that utilizes pixel intensity histograms (PIHs) of the observed images. Here, we apply the PIH method to the Quintuplet cluster and estimate the shape of its low-end IMF below the magnitude of completeness limit as set by conventional photometry. We found that the low-end IMF of the Quintuplet is consistent with that found for the Arches cluster—Kroupa MF, with a significant number of low-mass stars below $1 M_{\odot}$. We conclude that the most likely IMFs of the Quintuplet and the Arches clusters are not too different from the IMFs found in the Galactic disc. We also find that the observed PIHs and stellar number density profiles of both clusters are best reproduced when the clusters are assumed to be at three-dimensional distances of approximately 100 pc from the GC.

Key words: techniques: photometric – Galaxy: centre – galaxies: star clusters.

1 INTRODUCTION

The Quintuplet and Arches are two young ($\sim 2\text{--}4$ Myrs old), massive ($\sim 2 \times 10^4 M_{\odot}$), and compact (≤ 1 pc) star clusters that are located near (~ 30 pc in projection from) the Galactic center (GC; (Figer et al. 1999, 2002; Kim et al. 2000; Najarro et al. 2004; Martins et al. 2008; Espinoza, Selman & Melnick 2009)). Since the GC has unusual star-formation environments such as elevated temperatures and turbulent velocities in the molecular clouds, strong magnetic fields, and large tidal forces, these clusters have often been suspected to have had a shallower initial mass function (IMF) and/or an elevated low-mass cutoff (M_l) in the IMF. Thus, these clusters have been regarded as important targets for understanding the effects of the star-formation environment on the IMFs (Morris 1993).

Attempts to estimate the IMF of these extraordinary clusters have been carried out by high-resolution photometries using the infrared (IR) camera onboard the *Hubble Space Telescope* (*HST*), and also using a few ground IR telescopes with adaptive optics capabilities (Figer et al. 1999; Stolte et al. 2002, 2005; Kim et al. 2006; Espinoza, Selman & Melnick 2009; Hußmann et al. 2012;

Habibi et al. 2013). Yet, the stellar masses corresponding to the 50-percent completeness limit reach down to only $\sim 5 M_{\odot}$ for the Quintuplet and $1.3 M_{\odot}$ for the Arches (Kim et al. 2006; Hußmann et al. 2012), photometrically resolving stars fainter than this limit will have to wait until the next-generation IR space telescopes or extremely large ground telescopes are available.

The current photometric completeness limit for the Arches cluster was overcome by Shin & Kim (2015, Paper I hereafter), who devised a novel photometric method using the pixel intensity histograms (PIHs) of the observed image. The lower-end of the observed PIH contains information on the unresolved, faint stars. Paper I compared the PIHs between the observed images and the artificial images that were constructed with various synthetic luminosity functions (LFs) for the cluster. The synthetic LFs were constructed by combining the observed LF above the completeness limit and a model LF, which was converted from two different types of model mass functions (MFs): single power-law MFs and Kroupa MFs (Kroupa 2001). The fore/background stellar population towards the Arches cluster was built using the Milky Way star-count model of Wainscoat et al. (1992). They found that the low-end MF for the Arches cluster is consistent with the IMF found in the Galactic disc, a Kroupa IMF with a significant number of stars below $1 M_{\odot}$ that are not resolved by current IR telescopes.

* Email: jhshin.jhshin@gmail.com

† Corresponding author

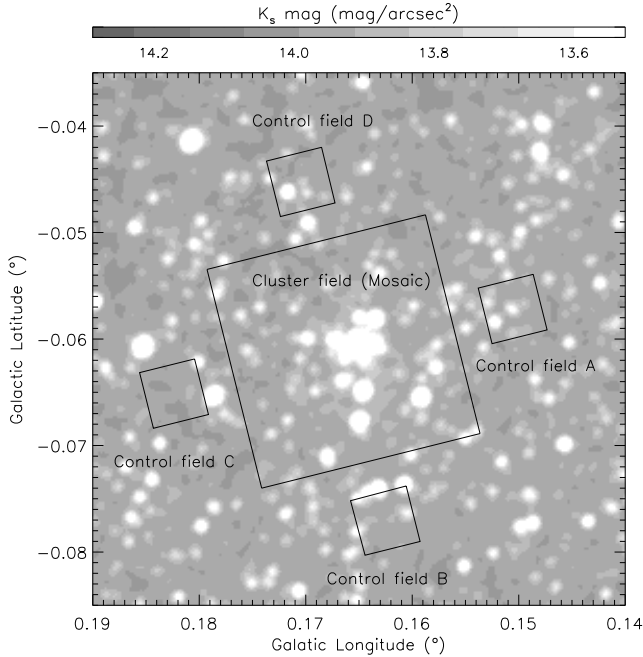


Figure 1. Locations and image sizes of the cluster field and the four control fields used in the present study. All fields were observed by the NICMOS2 camera onboard the *HST* (Figer et al. 1999). The cluster field was observed in a 4×4 mosaic pattern. The background is a K_s -band image from the 2MASS (Skrutskie et al. 2006).

The Quintuplet cluster is quite similar to the Arches cluster in several aspects (age, Galactocentric radius in projection, and initial total mass) except that the current stellar density of the Quintuplet is two orders of magnitude lower than that of the Arches. It is conceivable that the two clusters have been formed with similar initial conditions (total mass and size), but the Quintuplet, which was formed a few Myrs earlier, has evolved more dynamically, and thus currently has a lower stellar density (Kim et al. 2000). In the present paper, we apply the PIH method to the Quintuplet cluster to see if its lower-end IMF is also estimated to be similar to that of the Galactic disk, similar to the Arches.

This paper, a sequel to Paper I, is organized as follows. In §2, we describe the observational data used in the present study. We estimate the fore/background stellar population and background flux in the observed images towards the Quintuplet cluster in §3. §4 is devoted to tracing out the most plausible low-end MF of the Quintuplet cluster using the PIH method. A summary and discussion of the results are given in §5.

2 OBSERVATIONAL DATA AND PHOTOMETRY

The IR images of the Quintuplet cluster used in this study were obtained with the NICMOS2 camera onboard the *HST* on UT September 13/14, 1997 (Figer et al. 1999). The NICMOS2 camera has a field-of-view (FOV) of $19''.2 \times 19''.2$ and 256×256 pixels (each pixel covers $0''.076 \times 0''.076$ of

the sky). The cluster was observed in a mosaic-pattern of 4×4 , and four control fields were observed at a distance of $59''$ from the center of the cluster field (see Fig. 1). All image data were taken with F110W, F160W, and F205W filters, but the present study makes use of only the F205W images, as they suffer the smallest extinction. The exposure time of all F205W images used in the present study is 256 s.

Data were reduced using Space Telescope Institute (STScI) pipeline routines, and point spread function (PSF) photometry was performed using the DAOFIND and DAOPHOT packages (Stetson et al. 1987) within the Image Reduction and Analysis Facility (IRAF).¹ The conversion of the PSF flux into the Vega magnitude was done using the photometric keywords and zero-points announced on the STScI webpage².

Incomplete photometry for faint stars was corrected via recovery fractions; these are estimated for each 0.5 magnitude bin by planting artificial stars on the images. In our analyses in the forthcoming sections, only the portion of the observed LF whose recovery fraction is higher than 80% is used.

We adopted a distance modulus of 14.52 for the GC ($R_g = 8$ kpc; Reid 1993) and solar-metallicity isochrone at 4 Myr of the PARSEC model³ (Blessan et al. 2012) for the conversion between the stellar magnitude and the mass. The reddening value of each star was estimated from the color excess in the F160W–F205W colors and the extinction law of Nishiyama et al. (2006) with an assumption that all stars have the same intrinsic color of $(F160W - F205W)_0 = -0.05$ mag (Figer et al. 1999; Kim et al. 2006).

2.1 The Control Fields

Before applying the PIH method to the Quintuplet cluster, we first build the fore/background stellar LFs and estimate the background flux in the directions of the control fields.

For the magnitude bins brighter than a magnitude of 80% completeness, m_{80} , of each field (18.3, 18.1, 18.2, and 18.5 mag for control fields A, B, C, and D, respectively), we adopt the observed, completeness-corrected F205W LFs from each field. For the magnitude bins fainter than m_{80} , we construct model LFs using the star-count model of the Milky Way in the K band of Wainscoat et al. (1992).⁴ The K magnitudes of the stellar objects in the star-count model are reddened with an average extinction of 2.8 mag and observed standard deviations of 0.07, 0.08, 0.06, and 0.08 mag for the control fields A, B, C, and D, respectively. Here we assumed

¹ IRAF is distributed by the National Optical Astronomy Observatories, which are operated by the Association of Universities for Research in Astronomy, Inc., under cooperative agreement with the National Science Foundation.

² <http://www.stsci.edu/hst/nicmos/performance/photometry>

³ <http://stev.oapd.inaf.it/cmd>

⁴ We have shown in Paper I that our PIH analyses for the Arches cluster were not dependent on the choice of the Milky Way star-count model. We have tried the star-count model of Girardi et al. (2005) and Polido & Lépine (2013) in addition to the model of Wainscoat et al. (1992) for the Quintuplet cluster and have reached the same conclusion that the faint-end PIHs constructed from these models are nearly indistinguishable.

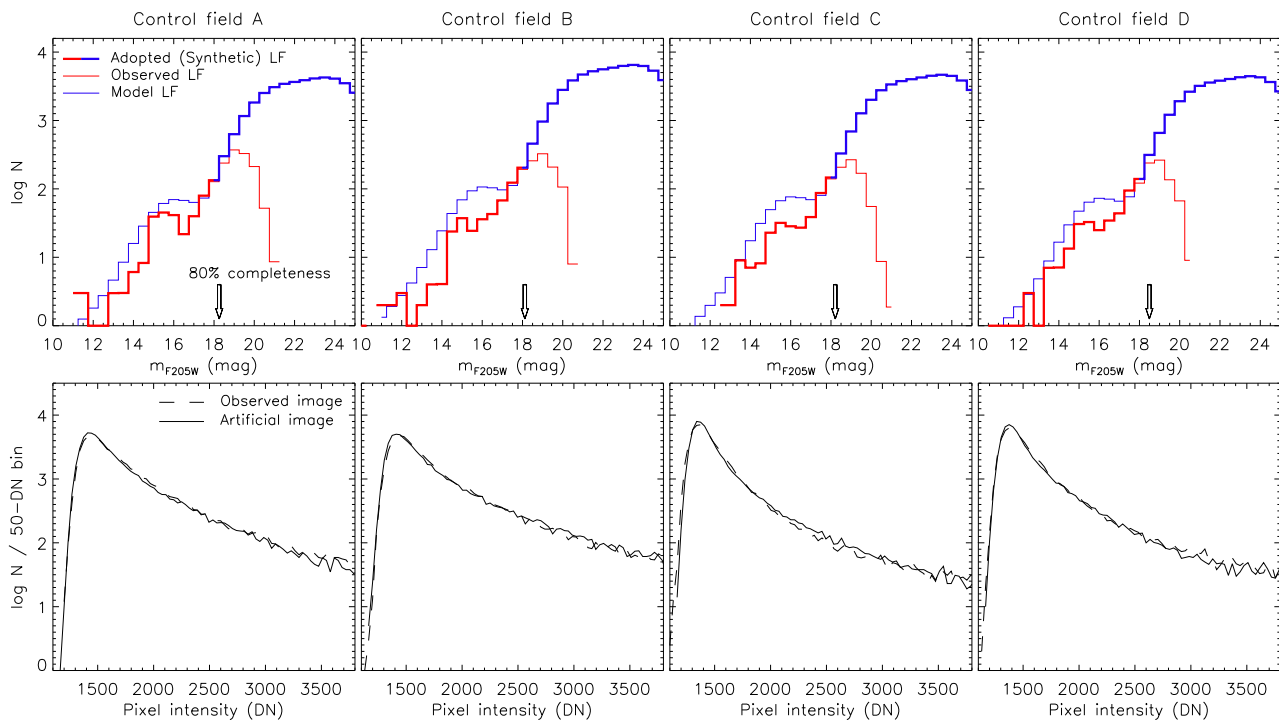


Figure 2. Luminosity functions (LFs) and pixel intensity histograms (PIHs) of the control fields A, B, C, and D. In the upper panels, the red lines are the completeness-corrected LFs from the observations, and the blue lines are the model LFs from the star-count model of Wainscoat et al. (1992). We vertically shifted the model LFs to match them with the observed LFs at m_{80} (arrows), then built the synthetic LFs (thick lines) by combining the observed LFs for the bright-part and the model LFs for the faint-part. The lower panels compare the observed PIHs (dashed lines) with the PIHs of the artificial images constructed from the corresponding synthetic LFs (solid lines). The histograms are the number of pixels for each 50-DN bin.

that the LFs in the K and F205W bands are adequately similar.

Since the star-count model may not be accurate towards the GC region due to a large and spatially varying extinction, the levels of the model LFs from the star-count model may be slightly different from the observed LFs near m_{80} . We found that the logarithmic model LFs of the control fields A, B, C, and D are 0.12, 0.26, 0.25, and 0.11 dex higher than the observed LFs at m_{80} respectively, thus we subtract these amounts from our model log LFs. These offset values are slightly smaller than those found for the control fields of the Arches cluster in Paper I.

We then construct the final synthetic LF, by merging the bright-part LF from the PSF photometry and the modified faint-part LF from the star-count model. The upper panels of Figure 2 show the completeness-corrected LFs from the observations (red lines), the model LFs modified (shifted vertically as described above) to match the observed LFs at m_{80} (blue lines), and the final synthetic LFs for the four control fields (thick lines).

Using these synthetic LFs for each control field, we construct artificial images following the same procedure described in Paper I, which can be summarized as follows: 1) artificial stars are planted in an empty artificial image at random locations using a set of 64 model PSFs, 2) the magnitude of the artificial stars are randomly chosen following the synthetic LF obtained above, 3) a dark current ($76.8 e^-$) and readout noise (standard deviation of $\sqrt{26} e^-$) are ap-

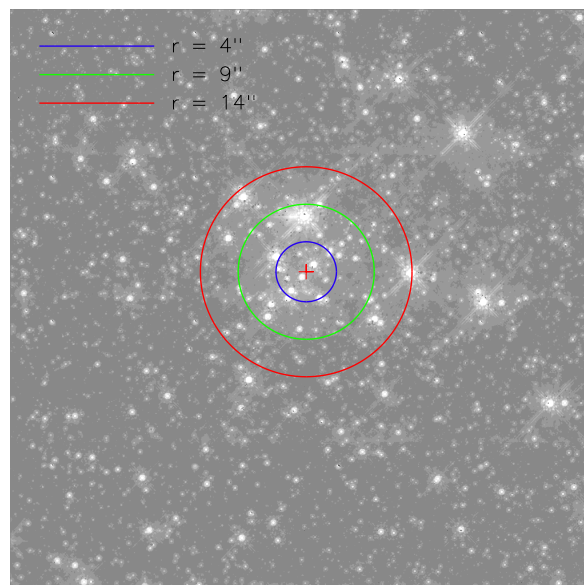


Figure 3. Cluster field image obtained with a F205W filter and the three annuli of 4, 9, and 14'' (corresponding to 0.16, 0.35, and 0.54 pc, respectively) from the cluster center, which is marked with a cross.

plied to the artificial image, and 4) a background flux of 1,225 DN (data number⁵) is added to the artificial image.

⁵ The gain, conversion between the electrons and the data number, of NICMOS2 camera is $5.4 e^-/\text{DN}$.

A background flux is composed of telescopic thermal noise, zodiacal light, external galactic sources, and cosmic IR background, making it rather difficult to estimate the background flux theoretically. As in Paper I, we estimated the amount of background flux toward the control fields by comparing our artificial images against the observed images. We found that adding a background flux of 1,225 DN results in a good match between the PIHs from the artificial and observed images for all four of the control fields (see the lower panels of Fig. 2). This amount is only slightly larger than that obtained for the control fields of the Arches cluster in Paper I, 1,190 DN.

The synthetic LFs and the background flux of 1,225 DN obtained for the four control fields here will also be used for the analyses of the cluster field, given in §4. The 95% confidence interval from our best-fit background flux of 1,225 DN is estimated to be ~ 10 DN. We find that our results from forthcoming PIH analyses are robust against the uncertainties in background flux estimation.

3 THE CLUSTER FIELD

The stellar number density and LF in the cluster field are highly position-dependent; the central region of the cluster is confusion limited by bright stars, while the outskirts of the cluster are limited by the foreground/background stars. For our analysis here, we use only the central region of the cluster field and divide it into three annuli of $0'' < r < 4''$, $4'' < r < 9''$, and $9'' < r < 14''$ (see Fig. 3). The position of the cluster center is defined to be the center of 100 brightest stars, R.A. = $17^{\text{h}}46^{\text{m}}15.24^{\text{s}}$ and dec. = $-28^{\circ}49'36.12''$. Unlike in Paper I, we make use of the innermost annulus ($0'' < r < 4''$), since the stellar number density of the Quintuplet is two orders of magnitude lower than that of the Arches, and the undesired contributions of bright stars to the PIHs are much less significant, even in the innermost region.

Our stellar photometry and completeness test result in $m_{80} = 14.4$ mag for $0'' < r < 4''$, 15.2 mag for $4'' < r < 9''$, and 16.8 mag for $9'' < r < 14''$. We construct the synthetic LF for the three cluster annuli by merging the bright-part LF from the PSF photometry and the faint-part LF from models. The latter consists of 1) the synthetic LF for the foreground/background stars, and 2) the LF converted from a model MF for the cluster stars. For the cluster model MF, two models are adopted: 1) single power-law MFs with various exponents (α) and lower mass limits (M_l)⁶ and 2) dynamically evolved Kroupa MFs (Kroupa 2001)⁷ with various M_l and tidal radii (R_t). We try the for a consistency check.

The artificial images for the three cluster annuli are constructed in the same procedure used for the control fields with a background flux of 1,225 DN, except that the magnitudes of the stellar objects are reddened with position-dependent extinction values obtained from our extinction

map. The averaged extinction of the cluster field is estimated to be 3.6 ± 0.2 mag for $0'' < r < 4''$, 3.4 ± 0.4 mag for $4'' < r < 9''$, and 3.0 ± 0.2 mag for $9'' < r < 14''$ (cf. 3.1 ± 0.2 mag obtained for $r < 12''$ by Figer et al. (1999) and 3.1 ± 0.5 mag for Wolf-Rayet stars in the inner part of the cluster by Liermann et al. (2010)). Since the area covered by each cluster annulus is rather small, unlike in the control fields, we used the magnitudes and positions of the actual observed stars when planting artificial stars brighter than m_{80} ; this was done in order to reduce the effects of random choices of magnitudes and positions of bright stars on the faint-end PIH.

3.1 Single Power-Law Mass Function

In this subsection, we describe our analyses performed with the single power-law MFs with various α and M_l values for the faint-part LF of the cluster. The upper panels of Figure 4 show a few sample synthetic LFs for the middle annulus ($4'' < r < 9''$), whose faint-part cluster LFs are from the MFs with three different α values (left panel), and three different M_l values (right panel). The lower panels of Figure 4 plot the PIHs of the observed images (dashed lines) and those of the artificial images constructed from the synthetic LFs in the corresponding upper panels (solid lines).

The lower panels show that the turnover intensity of the PIH depends on both the α and M_l values, although it is less sensitive on M_l than α . A few sample experiments shown in these panels already imply that the best-fit α and M_l for the middle annulus are around 2.1 and $0.1 M_{\odot}$, respectively. In order to quantitatively search for the best-fit α and M_l values, we minimize the χ^2 values between the PIHs from observed and artificial images. The number of DN bins used for the χ^2 test is 15.

The color map of χ^2 in the α - M_l space for the three cluster annuli are shown in panels a, b, and c of Figure 5. The minimum of χ^2 is near ($\alpha = 2.0_{-0.03}^{+0.03}$, $M_l = 0.03_{-0.01}^{+0.06} M_{\odot}$) for the inner annulus, ($\alpha = 2.0_{-0.02}^{+0.04}$, $M_l = 0.06_{-0.05}^{+0.04} M_{\odot}$) for the middle annulus, and ($\alpha = 2.0_{-0.02}^{+0.02}$, $M_l = 0.03_{-0.01}^{+0.07} M_{\odot}$) for the outer annulus (all the uncertainties in the present paper are 1-sigma confidence intervals). The χ^2 contours are elongated along the arc-like curves connecting the (large α , large M_l) and (small α , small M_l) corners of the α - M_l space. The sum of the three χ^2 values, which traces the best-fit α and M_l for the three annuli simultaneously, has a minimum at $\alpha = 2.0_{-0.03}^{+0.03}$ and $M_l = 0.06_{-0.02}^{+0.05} M_{\odot}$ (Fig. 5d).

Our analyses using single power-law MFs imply that the Quintuplet cluster has a significant amount of unresolved stars below its current photometric limit ($\sim 5 M_{\odot}$) and that the present-day MF of the Quintuplet is best reproduced with an α values that is smaller (shallower slope) than that of the Salpeter IMF.

3.2 Kroupa Mass Function

In this subsection, we adopt the Kroupa MFs (Kroupa 2001) with various M_l values as a more realistic initial MF of the cluster. We allowed them to dynamically evolve for 4 Myr using the anisotropic Fokker-Planck (FP) method described in Kim, Morris & Lee (1999) and Kim et al. (2000). Following these previous studies on the dynamics of the star clusters in

⁶ The function form of the single power-law MF is $dN(M) \propto M^{-\alpha} dM$ for $M > M_l$, where $dN(M)$ is the number of stars with masses between M and $M + dM$.

⁷ The Kroupa MF consists of three power-laws, $\alpha = 2.3$ for $M > 0.5 M_{\odot}$, $\alpha = 1.3$ for $0.08 < M/M_{\odot} < 0.5$, and $\alpha = 0.3$ for $M < 0.08 M_{\odot}$.

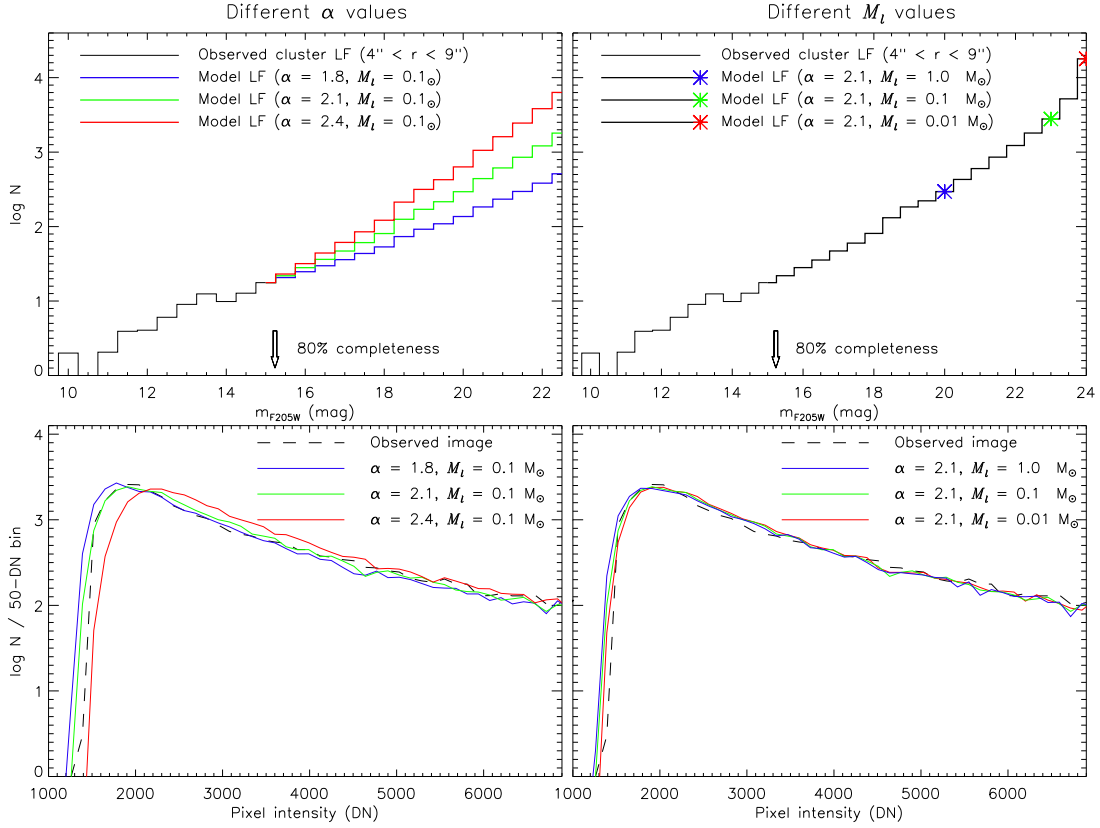


Figure 4. LFs and PIHs of the cluster field with different α (left panels) or M_t (right panels) values for the single power-law MFs. The model LFs, converted from the model MFs, are connected with the observed cluster LF at m_{80} (upper panels) to form the synthetic LFs. The PIHs of the artificial images constructed from the synthetic LFs are compared with the observed PIHs (lower panels).

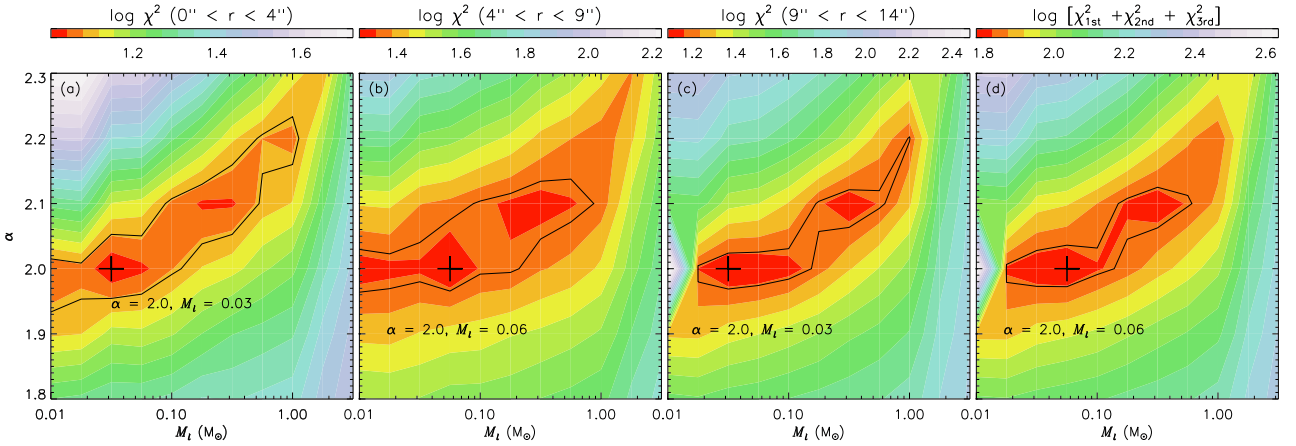


Figure 5. Color maps of χ^2 of the cluster field in the $\alpha - M_t$ space for the single power-law MF model. The first three panels are for $0'' < r < 4''$, $4'' < r < 9''$, and $9'' < r < 14''$ annuli, respectively, and the last panel is for the three annuli together. The minimum χ^2 points are marked with cross symbols. Black contours indicate the 95% confidence intervals from the minima.

the GC, we adopted the following initial conditions for the Quintuplet: density and velocity dispersion structures from the King model, a total mass of $2 \times 10^4 M_\odot$, upper mass boundary of $150 M_\odot$, and a King concentration parameter of 4.

One of the factors that affect the dynamical evolution

of a star cluster is the tidal radius of the cluster,

$$R_t = \left(\frac{M_{cl}}{2M_g} \right)^{1/3} R_g, \quad (1)$$

where M_{cl} is the cluster mass, and M_g is the Galactic mass inside a Galactocentric radius R_g . The R_g of the Quintuplet cluster is not certain, so we adopt three different

Table 1. Best-fit M_t values for the evolved Kroupa MF

Model	R_t [pc]	M_t [M_\odot]	χ^2				p-value [%]			
			0 – 4''	4 – 9''	9 – 14''	0 – 14''	0 – 4''	4 – 9''	9 – 14''	0 – 14''
1	1.1	$0.03^{+0.04}_{-0.01}$	22.56	25.04	12.32	59.91	6.79	3.41	58.09	4.48
2	1.7	$0.30^{+0.12}_{-0.12}$	16.54	25.85	10.65	53.04	28.12	2.71	71.35	14.03
3	2.3	$0.03^{+0.10}_{-0.01}$	14.83	27.71	17.43	59.97	39.00	1.55	23.39	4.43
4	2.5	$0.10^{+0.10}_{-0.07}$	14.41	24.16	10.08	48.64	41.99	4.39	75.61	25.61
5	3.5	$0.10^{+0.03}_{-0.02}$	13.98	26.86	9.32	50.16	45.09	2.01	81.02	21.06

Note—The p -value is the probability of having a χ^2 that is larger than the value obtained from our χ^2 test between the model and the observation, whose degree of freedom is 14 for each annulus of $0'' < r < 4''$, $4'' < r < 9''$, and $9'' < r < 14''$, and 42 for $0'' < r < 14''$.

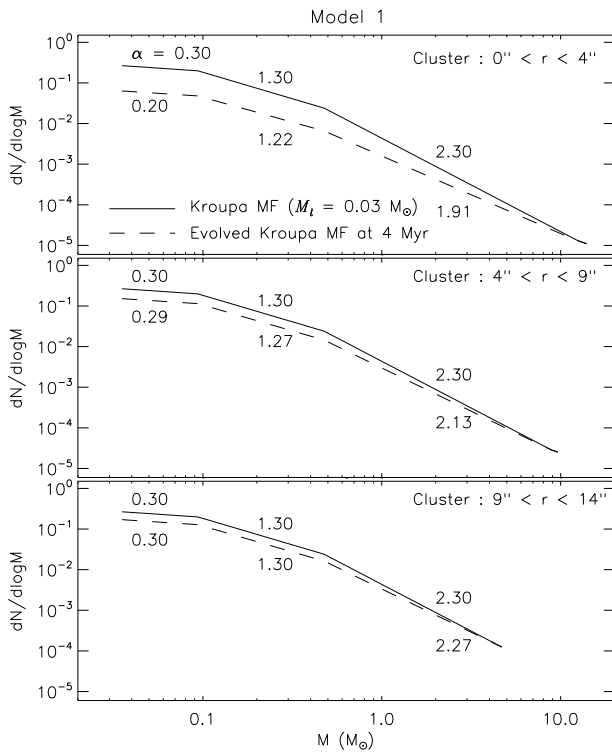


Figure 6. Original Kroupa MF (solid lines) and the dynamically evolved Kroupa MF at 4 Myr calculated using the Fokker-Planck model (dashed lines) below the masses that correspond to m_{80} for annuli of $0'' < r < 4''$ (top panel), $4'' < r < 9''$ (middle panel), and $9'' < r < 14''$ (bottom panel). The heights of the three MFs are adjusted to match at m_{80} . The original MF has an M_t of $0.03 M_\odot$, and the initial tidal radius of the cluster is 1.1 pc (Model 1).

values, 30 pc, 100 pc, and 200 pc. For the Galactic enclosed mass profile $M_g(R_g)$, we adopt two different models, those by [Genzel & Townes \(1987, GT87 hereafter\)](#) and [Laungardt, Zylka & Mezger \(2002, LZM02 hereafter\)](#). We try five different initial R_t values for the Quintuplet cluster: 1) 1.1 pc (Model 1; M_g of GT87 at $R_g = 30$ pc), 2) 1.7 pc (Model 2; M_g of LZM02 at $R_g = 30$ pc), 3) 2.3 pc (Model 3; M_g of GT87 at $R_g = 100$ pc), 4) 2.5 pc (Model 4; M_g of LZM02 at $R_g = 100$ pc), and 5) 3.5 pc (Model 5; M_g

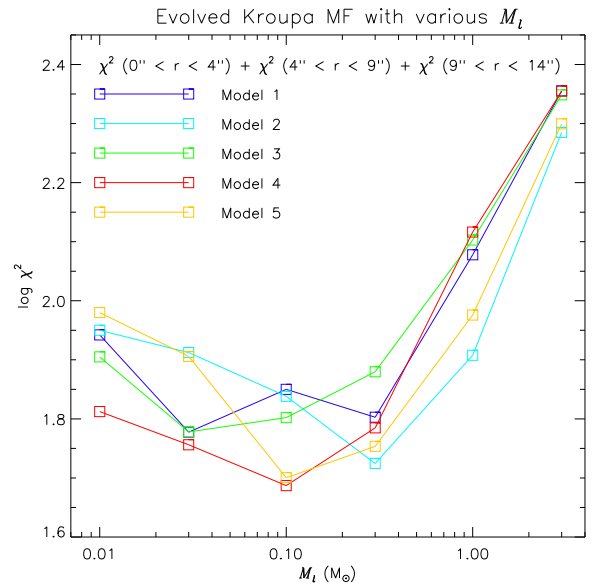


Figure 7. χ^2 values summed for all three annuli as functions of M_t for the evolved Kroupa MFs at 4 Myr. Different colors indicate different R_t models.

of GT87 and LZM02 at $R_g = 200$ pc; $M_g \sim 1.9 \times 10^9 M_\odot$ at $R_g = 200$ pc for both models).

Figure 6 compares the Kroupa IMF with $M_t = 0.03 M_\odot$ and $R_t = 1.1$ pc (Model 1) and its evolved MF at 4 Myr from our FP calculation. The MF at 4 Myr is shallower in the inner annulus, while it is steeper in the outer annulus; this is due to the mass segregation. Since the degree of mass segregation may differ for different values of M_t and R_t , the adopted MFs for each annulus depend on the M_t and R_t values of the cluster.

We construct the synthetic LFs and artificial PIHs for different M_t and R_t values in the same way as in §4.1. Figure 7 shows the logarithmic profiles of the summed χ^2 of the three annuli as a function of M_t for five different initial R_t values. The minimum χ^2 value is found at $M_t = 0.03^{+0.04}_{-0.01} M_\odot$ for $R_t = 1.1$ pc (Model 1), $M_t = 0.30^{+0.12}_{-0.12} M_\odot$ for $R_t = 1.7$ pc (Model 2), $M_t = 0.03^{+0.10}_{-0.01} M_\odot$ for $R_t = 2.3$ pc (Model 3), $M_t = 0.10^{+0.10}_{-0.07} M_\odot$ for $R_t = 2.5$ pc (Model 4), and $M_t = 0.10^{+0.03}_{-0.02} M_\odot$ for $R_t = 3.5$ pc (Model 5). The best-fit M_t values are found to be near or smaller than $0.3 M_\odot$ for a wide range of R_t models. Thus, it is almost certain

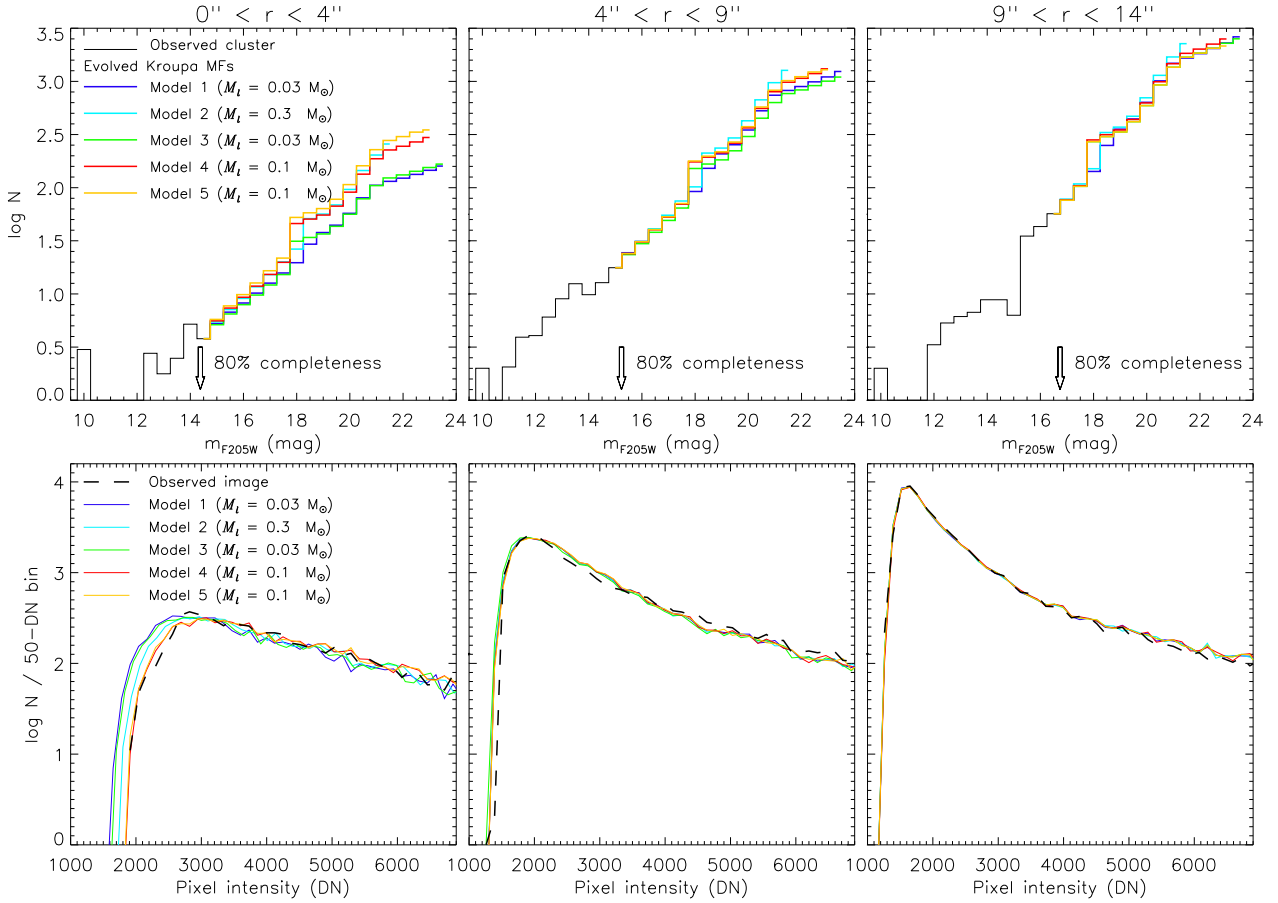


Figure 8. LFs and PIHs of the cluster field for the evolved Kroupa MFs with a best-fit M_t value for each R_t model. See the caption of Figure 4 for detailed descriptions.

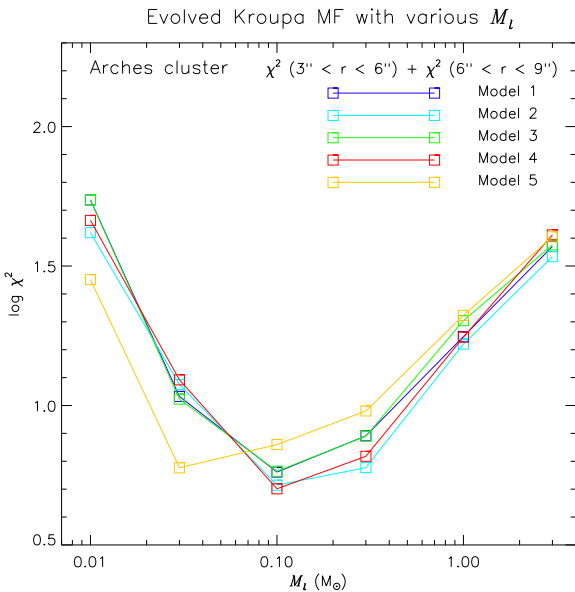


Figure 9. χ^2 values as functions of M_t for the evolved Kroupa MFs at 2 Myr for the *Arches cluster*. χ^2 values are summed for the annuli of $3'' < r < 6''$ and $6'' < r < 9''$. Different colors indicate different R_t models.

that a significant number of low-mass stars below the current photometric limit ($5 M_{\odot}$) of the cluster is required to match the observed PIH of the Quintuplet cluster. This is consistent with the findings of Paper I for the *Arches cluster* (only one R_t value was tried for the *Arches cluster* in Paper I, however). The χ^2 values and their p-values (statistical significance) for the best-fit parameter set of each R_t model are presented in Table 1. The p-value for the entire annuli ($0'' < r < 14''$) is acceptably high only for Model 4 and 5.

The synthetic LFs and PIHs constructed with the best-fit M_t value for each R_t model are shown in Figure 8. The sensitivity of the artificial PIH on R_t model is the largest in the inner annulus. The observed PIH in the inner annulus is best reproduced by the artificial PIHs of R_t Models 4 and 5 with $M_t = 0.1 M_{\odot}$. This can also be seen in Figure 7, where Models 4 and 5 have the two smallest χ^2 values among all the data points. This indicates that our analyses prefers the R_t Models 4 and 5, which experiences the least amount of mass segregation due to their larger R_t values (Models 4 and 5 have steeper LFs in the inner annulus than the other models; see the upper-left panel of Fig. 8).

In case of the *Arches cluster*, Paper I adopted only one initial value of R_t , 1.1 pc, because the PIH of the best-fit IMF obtained with that R_t value had a very good match with the observed PIH (the average χ^2 value for the two annuli was only ~ 0.7). In case of the *Quintuplet cluster*,

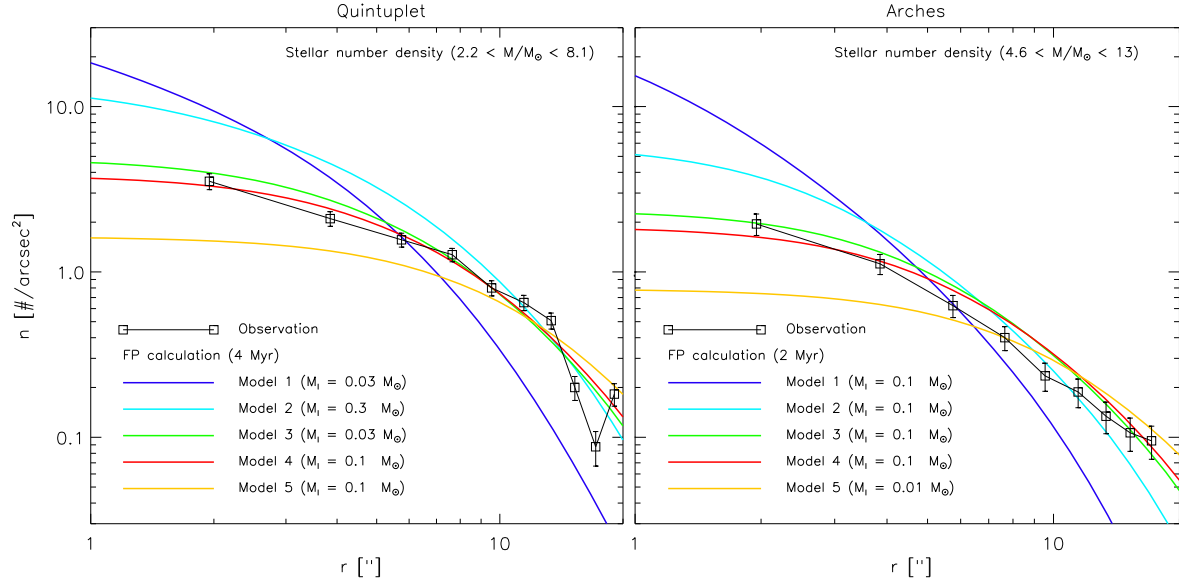


Figure 10. Stellar number density profiles of the Quintuplet and Arches clusters. Black lines are the completeness-corrected density profiles from the observations, and the colored lines are from our Fokker-Planck calculations. Stars within a certain mass range ($2.2 < M/M_{\odot} < 8.1$ for the Quintuplet and $4.6 < M/M_{\odot} < 13$ for the Arches) are considered for a comparison. Error bars represent the 1- σ uncertainties.

our initial trial for the R_t value, 1.1 pc, did not yield such small averages of χ^2 values. This is why we tried five different R_t values for the Quintuplet in the present study. We found that the initial value of R_t for the Quintuplet needs to be near or larger than 2.5 pc in order to result in as good a match as seen for the Arches.

The main cause of this difference between the Arches and the Quintuplet is the degree of dynamical evolution (or the age). The Quintuplet cluster has undergone greater mass segregation, thus the dependence of the LF on R_t is stronger in the Quintuplet. To check if this is indeed the case, we revisit the Arches cluster and perform the same analyses that we do in Paper I, i.e., for five different initial R_t values of 1.1, 1.7, 2.3, 2.5, and 3.5 pc. Figure 9 plots the R_t dependence of the total χ^2 (summed for the two annuli) as a function of M_i for the Arches cluster, and shows that the total χ^2 curve varies only slightly for different R_t values.

In order to see if some of our R_t models can be excluded, we compared the stellar number density profiles from observations to our FP calculations of model clusters with a Kroupa MF and the best-fit M_i value for each R_t model (see Fig. 10). For the number density profiles, we consider stellar mass ranges of $2.2 < M/M_{\odot} < 8.1$ and $4.6 < M/M_{\odot} < 13$, for the Quintuplet and Arches clusters, respectively. These mass ranges correspond to ± 1 mag from the magnitudes of 50% completeness at $r \sim 2''$, which are 16.8 mag and 15.9 mag. Here, the observed densities are the ones that are completeness-corrected by the estimated recovery fractions.

For both the Quintuplet and Arches clusters, the projected density profiles of R_t Models 1, 2, and 5 show significant deviations from the observations at the inner region ($r \lesssim 5''$), while those of Models 3 and 4 reproduce the reasonably well the observation for a wide radial range. Thus, the models with an initial R_t value smaller than 2 pc (R_g smaller than ~ 30 pc) or larger than 3.5 pc (R_g larger than

200 pc) can be excluded. The R_t range of 2–3.5 pc for these cluster is consistent with a recent study on the extended structure of the Arches cluster (Hosek et al. 2015), which found that the cluster does not exhibit any King-like tidal radius out to a radius of at least 2.8 pc. Among our five initial R_t models, only Model 4 agrees with the observed PIH and number density profile simultaneously, implying that both clusters are probably located approximately 100 pc away from the GC. The fact that both clusters have similar R_g estimates strengthens the notion that the two clusters were formed in the same or neighboring star-forming region(s) with similar initial masses, but at different epochs.

We also find that the evolved Kroupa MFs well reproduce the observed top-heavy MFs in the central regions of the Quintuplet and Arches clusters. Hußmann et al. (2012) estimate the MF slope at the center ($r < 0.5$ pc) of the Quintuplet to be $\alpha = 1.68$ for a mass range of $5 < M/M_{\odot} < 40$, whereas our Model 4 has $\alpha = 1.70 \pm 0.08$ for the same radial and mass range. The central MF slope for the Arches cluster is found to be 1.5–1.88 (Habibi et al. 2013; Espinoza, Selman & Melnick 2009), while our Model 4 gives $\alpha = 1.85 \pm 0.06$ for a mass range of $M > 10 M_{\odot}$ and radial range of $r < 0.2$ pc.

4 SUMMARY & DISCUSSION

Using the PIH method developed in Paper I, we estimated the shape of the low-end MF for the Quintuplet cluster, which is a young, compact star cluster located in the GC. We have adopted two model MFs for our PIH analyses, a single power-law MF and the Kroupa MF.

In the case of a single power-law MF, which was tried for a consistency check, the best-fits between the observed and model PIHs for $r < 14''$ were found at $\alpha = 2.0 \pm 0.03$ and

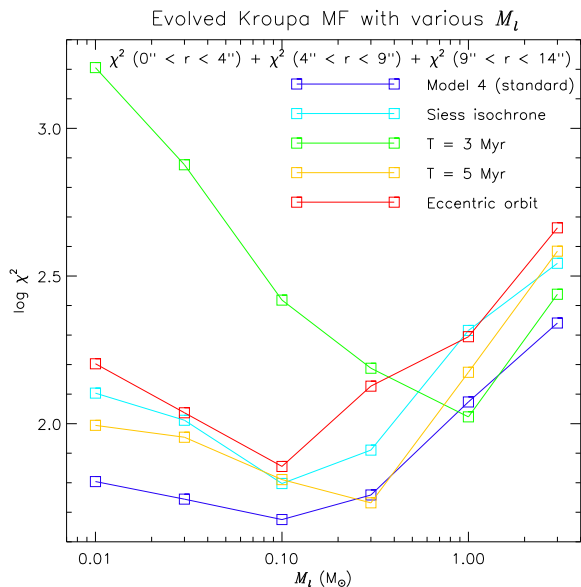


Figure 11. Comparison of χ^2 curves between our R_t model 4 (blue) and its variations (sky blue for the Siess isochrone model, yellow green and yellow for cluster ages of 3 Myr and 5 Myr, respectively, and red for the eccentric orbit).

$M_l = 0.06^{+0.05}_{-0.02} M_\odot$. This MF has a shallower α value than that of the Salpeter IMF, $\alpha = 2.35$, and has a lower M_l value than the current 50 % completeness limit of conventional photometry.

For the Kroupa MF model, we have dynamically evolved the MFs using the Fokker-Planck methods and compared them with the observed PIH. The best-fits between the observed and model PIHs for $r < 14''$ were found at $M_l = 0.03^{+0.04}_{-0.01} M_\odot$ for $R_t = 1.1$ pc, $M_l = 0.30^{+0.12}_{-0.12} M_\odot$ for $R_t = 1.7$ pc, $M_l = 0.03^{+0.10}_{-0.01} M_\odot$ for $R_t = 2.3$ pc, $M_l = 0.10^{+0.10}_{-0.07} M_\odot$ for $R_t = 2.5$ pc, and $M_l = 0.10^{+0.03}_{-0.02} M_\odot$ for $R_t = 3.5$ pc.

We found that the observed PIH of the Quintuplet is modeled reasonably well with the evolved Kroupa MF, and that the cluster has a significant number of faint stars that are not resolved by current IR telescopes. This implies that the IMF of the Quintuplet is not substantially different from the IMFs found in the Galactic disc, as is the case for the Arches cluster.

We also found that the observed PIHs and stellar number density profiles of both the Quintuplet and Arches clusters are best reproduced when the clusters are assumed to be at three-dimensional distances of ~ 100 pc from the GC. The fact that both clusters have similar R_g estimates strengthens the notion that the two clusters were formed in the same or neighboring star-forming region(s) with similar initial masses but at different epochs.

In order to check if our PIH analyses are dependent on the choice of isochrone, we have tried the Siess isochrones (Siess et al. 2000) in addition to the PARSEC model. Figure 11 compares the total χ^2 values of Model 4 for PARSEC with Siess isochrone models. The Siess model yields generally higher total χ^2 values than the PARSEC model, but results in the minimum χ^2 value at the same M_l as the PARSEC model. In case of a single power-law MF, we find that

our PIH analysis with the Siess model results in the χ^2 distribution very similar to that shown in Figure 5 except that the minimum χ^2 values are found at $M_l = 0.06^{+0.05}_{-0.02} M_\odot$ for the inner and outer annuli instead of at $0.03^{+0.07}_{-0.01} M_\odot$. Thus the locations of minimum χ^2 values are not sensitive to the choice of the isochrone.

The age of the Quintuplet is estimated to be 3-5 Myr (Figer et al. 1999). Inaccurate estimation of the cluster age can affect not only the mass-luminosity relation of the stars but also the degree of dynamical evolution (mass segregation and selective evaporation of lighter stars). In order to check the effect of cluster age on our results, we have tried cluster ages of 3 and 5 Myr for Model 4 in addition to 4 Myr, which was assumed throughout the paper. Figure 11 compares the total χ^2 values of Model 4 for cluster ages, 3, 4, and 5 Myr. The χ^2 profile of 5 Myr is quite similar to that of 4 Myr, but its minimum χ^2 is slightly larger than that of 4 Myr. The χ^2 profile of 3 Myr is significantly different from that of 4 Myr, and its minimum χ^2 is located at 10 times larger M_l than that of 4 Myr. However, the minimum χ^2 value is considerably higher than those of the 4 and 5 Myr cases, implying that our PIH analysis is much less consistent with a cluster age of 3 Myr.

Studies on the proper motion of the Quintuplet (Stolte et al. 2014) suggest that the cluster's orbit is probably elliptical rather than circular, whereas circular orbits are assumed for our FP calculations throughout the paper. The MF at a given radial bin in the cluster may be affected by the evolution of the tidal radius, which is determined by the orbit of the cluster. To see the impact of the non-circular orbit on our PIH analyses, we have tried an eccentric orbit of Stolte et al. (2014) for Model 4, whose current line-of-sight distance from the GC is 100 pc. Figure 11 shows that the shape of the χ^2 profile for the eccentric orbit is very similar to that for the circular orbit and that the χ^2 values for the eccentric orbit are larger at all M_l values. This demonstrates that the exact shape of the cluster orbit does not significantly affect our PIH analyses.

ACKNOWLEDGMENTS

We thank Pavel Kroupa for helpful discussion and comments. S.S.K. was supported by the National Research Foundation grant funded by the Ministry of Science, ICT and Future Planning of Korea (NRF-2014R1A2A1A11052367). J.S.'s work was supported by the International Cooperation and Exchange Program (No. 11450110400) funded by the National Natural Science Foundation of China (NSFC).

REFERENCES

- Blessan, A., Marigo, P., Girardi, L., Salasnich, B., Dal Cero, C., Rubele, S., & Nanni, A. 2012, MNRAS, 427, 127
 Espinoza, P., Selman, F. J., & Melnick, J. 2009, A&A, 501,563
 Figer, D. F., Kim, S. S., Morris, M., Serabyn, E., Rich, M., & McLean, I. S. 1999, ApJ, 525, 750
 Figer, D. F., Najarro, F., Gilmore, D., Morris, M., Kim, S. S., Serabyn, E., McLean, I. S., Gilbert, A. M., Graham, J. R., Larkin, J. E., Levenson, N. A., & Teplitz, H. I. 2002, ApJ, 581, 258
 Genzel, R., & Townes, C. H. 1987, ARA&A, 25, 377

- Girardi, L., Groenewegen, M. A. T., Hatziminaoglou, E., & da Costa, L. 2005, *A&A*, 436, 895
- Habibi, M., Stolte, a., Brandner, W., Hußmann, B., & Motohara, K. 2013, *A&A*, 556, 26
- Hosek, M. W., Lu, J. R., Anderson, J., Ghez, A. M., Morris, M. R., Clarkson, W. I. 2015, arXiv:1509.04716
- Hußmann, B., Stolte, A., Brandner, W., Gennaro, M., & Liermann, A. 2012, *A&A*, 540, 57
- Kim, S. S., Figer, D. F., Lee, H. M., & Morris, M. 2000, *ApJ*, 545, 301
- Kim, S. S., Figer, D. F., Kudritzki, R. P., & Najarro, F. 2006, *ApJ*, 653, L113
- Kim, S. S., Morris, M., & Lee, H. M. 1999, *ApJ*, 525, 228
- Kroupa, P. 2001, *MNRAS*, 322, 231
- Launhardt, R., Zylka, R., & Mezger, P. G. 2002, *A&A*, 384, 112
- Liermann, A., Hammann, W.-R., Oskinova, L. M., Todt, H., & Butler, K. 2010, *A&A*, 524, 82
- Martins, F., Hillier, D. J., Paumard, T., Eisenhauer, F., Ott, T., & Genzel, R. 2008, *A&A*, 478, 219
- Morris, M. 1993, *ApJ*, 408, 496
- Najarro, F., Figer, D. F., Hillier, D. J., & Kudritzki, R. P. 2004, *ApJ*, 611, L105
- Nishiyama, S., Nagata, T., Kysakabe, N., Matsunaga, N., Naoi, T., Kato, D., Nagashima, C., Sugitani, K., Tamura, M., Tanabé, T., & Sato, S. 2006, *ApJ*, 638, 839
- Polido, P., Jablonski, F., & Lépine, J. R. D. 2013, *ApJ*, 778, 32
- Reid, M. J. 1993, *A&A*, 31, 345
- Shin, J. & Kim, S. S. 2015, *MNRAS*, 447, 366 (Paper I)
- Siess, L., Dufour, E., & Forestinim, M. 2000, *A&A*, 358, 593
- Skrutskie, M. F. et al. 2006, *AJ*, 131, 1163
- Stetson, P. B., Hesser, J. E., Smith, G. H., Vandenberg, D. A., & Bolte, M. 1987, *AJ*, 97, 1360
- Stolte, A., Grebel, E. K., Brandner, W., & Figer, D. F. 2002, *A&A*, 394, 459
- Stolte, A., Brandner, W., Grebel, E., Lenzen, R., & Lagrange, A. 2005, *ApJ*, 628, L113
- Stolte, A., Hußmann, B., Morris, M. R., Ghez, A. M., Brandner, W., Lu, J. R., Clarkson, W. I., Habibi, M., & Matthews, K. 2014, *ApJ*, 789, 115
- Wainscoat, R. J., Cohen, M., Volk, K., Walker, H. J., & Schwartz, D. E. 1992, *ApJS*, 83, 111